Vol. 679: 19–30, 2021
https://doi.org/10.3354/meps13883

MARINE ECOLOGY PROGRESS SERIES
Mar Ecol Prog Ser

Published November 25

A bio-optical model for the estimation of chlorophyll *a* using animal-borne instruments in an optically complex ecosystem

B. V. R. Nowak*, W. D. Bowen, D. C. Lidgard, S. J. Iverson

Department of Biology, Dalhousie University, Halifax, Nova Scotia B3H 4JI, Canada

ABSTRACT: Studies using marine animals instrumented with biologging devices to estimate phytoplankton biomass have typically omitted continental shelf regions due to the confounding effects of optically active constituents other than phytoplankton present. The lack of algorithms for these regions is problematic, as they are some of the most biologically productive in the world and are often inhabited by the species of interest. We developed a bio-optical model to estimate chlorophyll *a* concentration (chl *a*) using light attenuation (*LA*) measured using a standard oceanographic instrument in an optically complex water body that is applicable to data collected by animal-borne devices. To achieve this, we conducted a replicated experiment to compare measurements made using time–depth–light recorders (TDLRs) to those of a standard oceanographic instrument (the HyperPro) in an adjacent water body, the Bedford Basin, Nova Scotia, Canada. Measurements of *LA* made by TDLRs were comparable to those of the HyperPro at-depth. The best supported bio-optical model for the estimation of chl *a* included both *LA* measured by the HyperPro and season as a fixed effect. The use of animal-borne devices to collect subsurface chl *a* data not only provides an opportunity to collect valuable oceanographic data but also allows for the exploration of broader ecological questions relating to the influence of primary productivity on the movement patterns of wide-ranging marine species.

KEY WORDS: Chlorophyll *a* · Light attenuation · Continental shelf · Biologging · Animal-borne sensors · Bedford Basin

1. INTRODUCTION

The oceans provide nearly half of the earth's net primary productivity, with phytoplankton playing a fundamental role in global carbon cycling (Falkowski et al. 1998, Field et al. 1998). Thus, monitoring the spatial and temporal patterns of phytoplankton biomass is of considerable interest, particularly in the face of climate change (Sarmiento et al. 1998, Blondeau-Patissier et al. 2014, Behrenfeld et al. 2016, Moore et al. 2018). Marine primary productivity is typically inferred from phytoplankton biomass, expressed as phytoplankton abundance (cells m^{-3}), organic carbon concentration (mg m^{-3}), or chlorophyll *a* (chl *a*) concentration (mg m^{-3}). However, chl *a* is the most used proxy for phytoplankton biomass (Cullen 1982, Behrenfeld & Falkowski 1997). Measurements of chl *a* are traditionally made from research vessels, moorings (Stabeno et al. 1998), floats (Riser et al. 2016), or autonomous underwater vehicles (AUVs; Wynn et al. 2014). These platforms are generally costly and often do not provide data at large spatial (and sometimes temporal) scales.

Remote sensing of chl *a* using ocean colour algorithms has been used to monitor primary productivity patterns, including the detection of phytoplankton blooms (Blondeau-Patissier et al. 2014). Nevertheless, there are several limitations associated with re-

*Corresponding author: bernadette.nowak@dal.ca

mote sensing, including missing data due to cloud cover or heavy ice conditions (Ackerman et al. 1998, Friedl et al. 2010) and the challenges of atmospheric correction in optically complex waters (Moses et al. 2009). For these reasons, data are often patchy, both spatially and temporally. Remote sensing is also restricted to the first optical depth, below which, subsurface chl *a* may be missed (Cullen 1982, Cullen & Lewis 1995).

Several studies have shown that instrumented, large marine species can serve as 'bioprobes' to collect valuable oceanographic data throughout their ranges (e.g. Hooker & Boyd 2003, Padman et al. 2010, Roquet et al. 2014). The use of animal-borne sensors on wide-ranging, deep-diving species is an alternative method for the remote estimation of chl *a* (e.g. Teo et al. 2009, Jaud et al. 2012, Guinet et al. 2013, Bayle et al. 2015, O'Toole et al. 2014). This approach can provide fine-scale estimates of chl *a* within the water column along an animal's path. Two types of animal-borne instruments have been used to estimate chl *a*: miniaturized fluorometers (e.g. Xing et al. 2012, Guinet et al. 2013) and light level (*LL*) sensors embedded in biologging tags (e.g. Teo et al. 2009, Jaud et al. 2012, O'Toole et al. 2014). The use of miniaturized fluorometers is burdened by several constraints, including the need to correct for non-photochemical quenching and discrepancies related to spatio–temporal variability in phytoplankton photophysiology and community composition (Behrenfeld et al. 2009, Xing et al. 2012, Lander et al. 2015).

An alternative method is to repurpose *LL* data collected by light-based geolocation tags to measure light attenuation (*LA*; m^{-1}) within the water column. The diffuse attenuation coefficient of downwelling irradiance (k_d; m^{-1}) is an apparent optical property that is standard in both subsurface oceanographic sampling and remote sensing and is commonly used to estimate chl *a* (e.g. Lee et al. 2005a). k_d can be calculated by linearly regressing log-transformed downwelling irradiance (E_d; W m^{-2}) with depth (Kirk 1994, Lee et al. 2005b). As *LL* is an approximate conversion of log-transformed light intensity (W cm^{-2}) and thus E_d specific to these devices, *LA* provides a relative measure of k_d. Recent work using animal-borne instruments has highlighted the use of *LA* to estimate chl *a* (O'Toole et al. 2014). These biologging devices use cosine *LL* sensors and are typically instrumented on the heads of animals (Lidgard et al. 2014), such that they are facing upwards during the ascent phase of dives when *LL* data are used (Jaud et al. 2012). They are also equipped with blue-range transmittance filters to maximize light detection at-depth, as the attenuation of pure water is at a minimum in this range (Morel & Prieur 1977, Morel & Maritorena 2001). The majority of *LA* attributable to phytoplankton also falls within this range, making these devices suitable for inferring chl *a* (Morel & Prieur 1977, Morel & Maritorena 2001).

In open ocean waters, phytoplankton and optically active by-products that covary with phytoplankton dominate *LA* in the water column (referred to as Case 1 waters) (Smith & Baker 1978, Baker & Smith 1982, Morel et al. 2006). This has allowed for the development of empirical global algorithms for the estimation of chl *a* (Morel & Prieur 1977, O'Reilly et al. 1998, Morel & Maritorena 2001, Lee et al. 2005a). However, these algorithms may not be suitable where the pigment concentrations of the local phytoplankton community differ or where substantial non-algal optically active constituents are present (Darecki et al. 2003, Siegel et al. 2005, Moore et al. 2009). Continental shelf waters are shallow (typically <200 m) with proximity to landmasses. As a result, freshwater inputs often contain coloured dissolved organic matter (CDOM) that may influence their optical properties. These exogenous sources of CDOM vary independently from phytoplankton biomass (referred to as Case 2 waters) (Smith & Baker 1978, Baker & Smith 1982). The absorption of light by CDOM poses a challenge as it falls within the same range of the spectrum as that of chl *a* (Bricaud et al. 1981).

To date, studies involving the use of biologging tags to estimate chl *a* have omitted continental shelf regions due to the confounding effects of optically active constituents other than phytoplankton (Jaud et al. 2012). Development of predictive algorithms to accommodate the presence of both Case 1 and Case 2 waters has been a major challenge for both remote sensing satellites and AUVs (Devred et al. 2005, Fuentes-Yaco et al. 2015, Beck 2016). As noted above, the lack of Case 2 algorithms is problematic in the context of animal-borne instruments, as the species of interest often forage in coastal or continental shelf areas (e.g. Campagna et al. 2007, Bailleul et al. 2010, Hindell et al. 2016). Continental shelves are important areas in terms of monitoring phytoplankton biomass, as the primary productivity on continental shelves exceeds that of the open ocean, especially at higher latitudes (Behrenfeld et al. 2009). Thus, locally validated algorithms for the estimation of chl *a* specific to Case 2 ecosystems are needed.

The Scotian Shelf is a highly productive continental shelf ecosystem. It is home to the world's largest

population of grey seals *Halichoerus grypus*, with an increasing population currently estimated at >424 000 individuals (Hammill et al. 2017). Grey seals are primarily benthic foragers, diving frequently to near the ocean floor, making this species a good candidate for monitoring chl *a* throughout the water column (Thompson et al. 1991, Beck et al. 2003). The instrumentation of grey seals would be especially useful, given the maximum chl *a* is found below the first optical depth across the Scotian Shelf (Ross et al. 2017). Since the movements of grey seals have been intensively studied in this region, they represent a rich source of *LL* data for the estimation of phytoplankton biomass. Between 2009 and 2015, nearly 120 grey seals were instrumented with time–depth–light recorders (TDLRs).

The development of regionally specific bio-optical models must be validated against *in situ* measurements of chl *a*. Approaches to validation have included deployment of biologging devices together with measurements of chl *a* along a cruise track (Teo et al. 2009) or using satellite-derived chl *a* estimates that are concurrent with animal locations (O'Toole et al. 2014). The logistical challenges of a ship-based approach and the difficulty of pairing remote sensing data with grey seal locations would result in insufficient observations to develop a long-term predictive algorithm over multiple seasons and years. Therefore, we conducted a replicated experiment in an adjacent water body, the Bedford Basin, Nova Scotia, Canada. The Bedford Basin is a coastal inlet connected to the Scotian Shelf by a long (10 km), shallow (20 m) sill (Li & Harrison 2008). These waters are part of the same large-scale physical regime (Loder et al. 1998), and analysis of temperature data has shown that the Bedford Basin experiences the same environmental perturbations as the continental shelf (Bundy et al. 2014). The Bedford Basin exhibits the same climatology as the Scotian Shelf, losing ecological autonomy after only 3 d (Lewis & Platt 1982, Li & Dickie 2001). Water exchange between the Bedford Basin and Scotian Shelf occurs via Ekman transport and is heavily influenced by the Nova Scotia Current (Greenberg et al. 1997, Shan et al. 2011, Shan & Sheng 2012, Dever et al. 2016). Like coastal and shallow areas of the Scotian Shelf, the Bedford Basin is optically complex and can be classified as a Case 2 water body (Song et al. 2010, Bundy et al. 2014). Results of multi-year time series analyses within the Bedford Basin and across the Scotian Shelf indicate that both nutrient concentrations and phytoplankton abundances are within the same ranges (Platt et al. 1972, Petrie et al. 1999, Li et al. 2006, 2010). The objective of this study was to develop a long-term bio-optical model to estimate chl *a* using *LA* measurements made by a standard oceanographic instrument that is applicable to data collected by instrumented grey seals in the Case 2 waters of the Scotian Shelf.

2. MATERIALS AND METHODS

2.1. Experimental procedure

This study took advantage of a weekly sampling regime for several oceanographic properties in the Bedford Basin, allowing for replicate observations within a single experimental system. Sampling and sample processing were performed between 2009 and 2015 by the Marine Environmental Observation Prediction and Response Network (MEOPAR) and Dalhousie University in conjunction with the Department of Fisheries and Oceans Canada as part of the Bedford Basin Monitoring Program at the Compass Buoy Station (44° 41′ 37″ N, 63° 38′ 25″ W) (Li & Dickie 2001). For further details on the methods for sampling and sample processing of these oceanographic data, the authors recommend contacting Coastal Environmental Observation Technology and Research (www.ceotr.ca/).

Niskin bottle collections were made at 1, 5, and 10 m depths to obtain quantitative measurements of subsurface chl *a* for inclusion in the bio-optical model. Samples were prepared by passing 39 ml through 25 mm glass fibre filters and then extracted in 90% acetone for 24 h; 3 replicates were performed for each depth. Samples were then processed using the Welschmeyer non-acidification technique (Welschmeyer 1994) to account for interfering pigments and then read on 2 Turner Designs Fluorometers (www.turnerdesigns.com) with a 436/685 filter pair and range of 0 to 300 ± 0.025 mg m^{-3}. These samples were also processed for the measurement of spectral CDOM absorbance (A_{CDOM}) to explore the relationship of non-algal optically active constituents with *LA* measurements. A_{CDOM} was measured by filtration through a nucleopore filter and run on a Cary spectrophotometer in a 10 cm long cuvette. Filtrate was kept in a glass bottle, the filter was discarded with the sample, and nanopure was used to blank. Measurements were taken within a spectral range of 250 to 800 nm, and one replicate was performed for each depth.

A micro CTD (conductivity–temperature–depth) system (AML Oceanographic, www.amloceanographic

.com) mounted with a WET Labs ECO Triplet-*W* fluorometer (Sea-Bird Scientific, www.seabird.com) was lowered at a rate of 0.5 m s^{-1} to a maximum depth of 60 m. The fluorometer measured chl *a* fluorescence (F_{chl}) intensity using a 470/695 filter pair at a frequency of 1 Hz and was binned at a resolution of 0.5 m. Since the fluorometer was not calibrated to measure the concentrations of chl *a*, data are instead reported in volts (V) and serve as both a useful proxy and validation method for Niskin bottle chl *a* measurements.

An optical profiling platform equipped with a Satlantic hyperspectral OCR-3000, referred to as the HyperPro (Sea-Bird Scientific, www.seabird.com), was deployed immediately after the CTD system to measure spectral E_d used in the estimation of *LA* for the bio-optical model. Measurements were made using a 256-channel silicon photodiode array with a spectral range of 350 to 800 nm at a resolution of 10 ± 0.3 nm with less than 0.001 W m^{-2} of stray light detected. Three casts were performed on each weekly sampling date: the first to a maximum depth of 60 m, followed by 2 casts to depths where usable light was no longer detected.

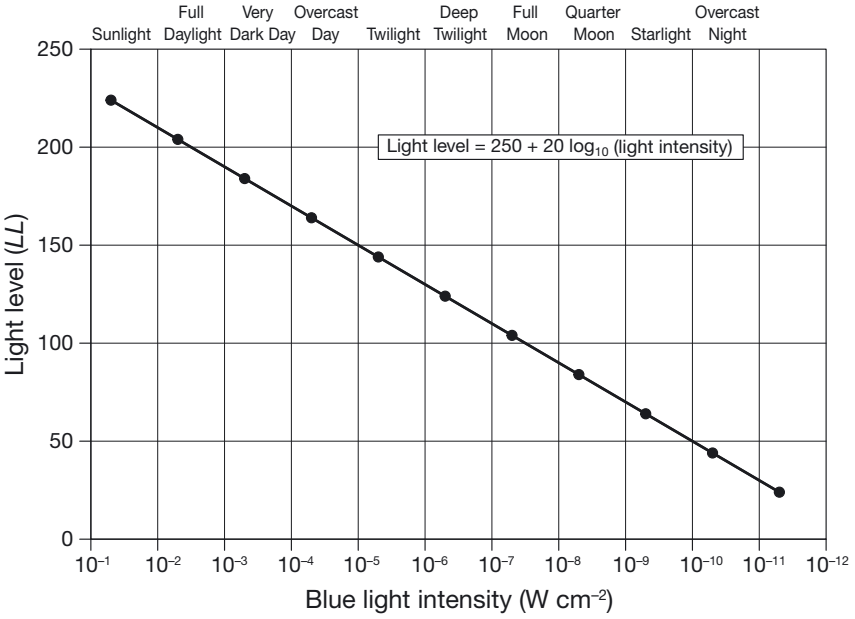

Fig. 1. Logarithmic conversion of light intensity (W cm^{-2}) within the blue range of the visible spectrum to light level (*LL*) values measured using Mk10-AF™ GPS tags (Wildlife Computers, www.wildlifecomputers.com)

To compare *LA* measurements made using TDLRs and the HyperPro, on 12 of the weekly sampling dates over spring and early summer of 2012, 5 TDLRs (Mk10-AF Fastloc™ GPS tags, Wildlife Computers, www.wildlifecomputers.com) (serial numbers 11A0091, 11A0214, 11A0254, 11A0256, 11A0257) were attached to the CTD system, such that the light sensors were unobstructed. As we wanted the bio-optical model of chl *a* to be valid for data collected by grey seals inhabiting the Scotian Shelf, we used the same model of TDLRs instrumented on free-ranging seals. Temperature was measured using a fast-response external thermistor with a range of –40 to 60°C at a resolution of 0.05 ± 0.1°C. Depth was measured within a range of 0 to 1000 m at a resolution of 0.5 m ± 1% of depth reading. The *LL* sensor is comprised of a Hamamatsu silicon S2387 photodiode and a blue window transmittance filter, resulting in a peak sensitivity of 465 nm with a range of 400 to 490 nm and half band width of 50 nm at 420 and 470 nm (Vacquié-Garcia et al. 2017). Sensitivity between these half-band frequencies is non-normal. *LL* data are collected within a range of 25 to 225 units, which corresponds approximately to 5×10^{-12} to 5×10^{-2} W cm^{-2}. Calibrations were performed by instrument manufacturers at light intensity values of 10^{-5}, 10^{-7}, and 10^{-9} W cm^{-2}, resulting in *LL*s of 150, 110, and 70, respectively (Fig. 1). Deviations in *LL* profiles of TDLRs were evident at the surface for 2 of the deployment dates and were removed from these analyses; it is possible that these were due to the presence of passing clouds (Beck 2016).

2.2. Data analysis

Data analyses were performed using R statistical software (version 3.4.4; R Core Team, 2018). Niskin bottle samples provided the only quantitative chl *a* data for this study; however, they were limited to a maximum sampling depth of 12 m. Thus, data included in the validation of both chl *a* and *LA* and the bio-optical model were restricted to the top 12 m (referred to as the near-surface depth). To obtain the average chl *a* over this depth, comparable to per meter values of *LA*, data were numerically integrated using the midpoint Reimann sum. The widths of the rectangle bases were used as weights for the equation:

$$\text{chl } a = \frac{1}{6}\,\text{chl } a_1 + \frac{1}{2}\,\text{chl } a_5 + \frac{1}{3}\,\text{chl } a_{10} \quad (1)$$

using measurements at depths 1, 5, and 10 m. Prior to analysis, A_{CDOM} was restricted to a wavelength of

465 nm, $A_{CDOM}(465)$, corresponding to the peak sensitivity of TDLRs. A baseline correction was performed on these data by subtracting $A_{CDOM}(685)$ from that of $A_{CDOM}(465)$ (Helms et al. 2008, Xie et al. 2012). The spectral absorption coefficient, $a_{CDOM}(465)$ (m^{-1}) was then calculated using the following equation:

$$a_{CDOM}(465) = 2.303 A_{CDOM}(465) / l \quad (2)$$

where $A_{CDOM}(465)$ is the absorbance at 465 nm and l is the path length of 0.1 m (Xie et al. 2012). As with measurements of chl *a*, mean values of a_{CDOM} were calculated for each sampling date using the midpoint Reimann sum with the widths of rectangle bases as weights:

$$a_{CDOM}(465) = \frac{1}{6} a_{CDOM}(465)_1 + \frac{1}{2} a_{CDOM}(465)_5 + \frac{1}{3} a_{CDOM}(465)_{10} \quad (3)$$

On dates where $a_{CDOM}(465)$ data were incomplete due to sampling errors, depths were re-weighted to reflect available data.

F_{chl} served as both a proxy and validation measurement for chl *a* as sampling occurred at a higher frequency, providing more data and thus a more accurate representation of the water column. The correction for non-photochemical quenching was performed prior to analysis of F_{chl} by extrapolating the maximum fluorescence intensity between the mixed-layer depth (MLD) and the surface (Xing et al. 2012, Guinet et al. 2013). The MLD was determined by estimating the depth of the thermocline using the finite-depth criterion method with temperature data collected by the CTD (de Boyer Montégut et al. 2004). This method is particularly well suited for this region, as seasonal stratification is driven by temperature gradients (Li & Harrison 2008). A criterion value of 0.5°C was chosen as it has been used in both the global ocean and specific to the North Atlantic (de Boyer Montégut et al. 2004). A reference depth of 15 m was used to remove the influence of diurnal increases in surface temperature, as they were observed below 10 m on several dates of the study (Xing et al. 2012). The validation of temperature data for these devices was performed in a previous study (Simmons et al. 2009). Average F_{chl} within the near-surface waters (i.e. 12 m) was then calculated by numerical integration using the composite trapezoidal rule with the freely available R package *caTools* (Blain et al. 2013, Tuszynski 2014).

Light intensity is approximately converted onboard TDLRs to a 3-digit *LL* value specific to the manufacturers (Fig. 1) to enhance resolution at lower light intensities using the equation:

$$LL = 250 + 20 \log_{10} (\text{light intensity}) \quad (4)$$

E_d measurements collected by the HyperPro were taken at 465 nm, corresponding to the peak sensitivity of TDLRs. E_d data were then converted to *LL* (Eq. 4) to standardize comparisons between the HyperPro and TDLRs and validate the application of the multi-year bio-optical model to grey seal TDLR data. *LA* was calculated for both the HyperPro (LA_{HP}) and TDLRs (LA_{TDLR}) by linearly regressing vertical *LL* profiles (Lee et al. 2005b). LA_{HP} and LA_{TDLR} were then compared using the root mean square error (RMSE) and mean absolute percentage error (MAPE) for each of the 10 sampling dates TDLRs were deployed using the equations:

$$RMSE = \sqrt{\frac{1}{10} \sum_{i=1}^{10} (LA_{TDLR,\,i} - LA_{HP,\,i})^2} \quad (5)$$

$$MAPE = \frac{100}{10} \sum_{i=1}^{10} \left| \frac{LA_{TDLR,\,i} - LA_{HP,\,i}}{LA_{TDLR,\,i}} \right| \quad (6)$$

For the 10 sampling dates where all data were available, estimates of chl *a* and other indicators of optically active constituents, $a_{CDOM}(465)$ and F_{chl}, were compared to both LA_{HP} and LA_{TDLR} to explore the nature of their relationships within the near-surface waters of this optically complex system.

Between 2010 and 2015, weekly measurements of chl *a* from Niskin bottle samples and LA_{HP} within the near-surface waters were used to develop a bio-optical model for the intended purpose of estimating chl *a* using *LL* data collected *in situ* by grey seals during this period. LA_{HP} were estimated using data from all 3 casts. Erroneous LA_{HP} estimates were identified as those with $R^2 < 0.80$; 28 profiles were removed. Data were limited to dates on which both chl *a* and LA_{HP} were available and as no chl *a* data were collected in 2009, 165 profiles remained for analysis. The bio-optical model for the estimation of chl *a* using LA_{HP} was constructed using a generalized least squares regression (GLS) to minimize the sum of squared residuals and predict one variable from the other. To meet the assumptions of a linear regression, both chl *a* and LA_{HP} were log-transformed and a continuous first-order autoregressive structure was specified on ordered observations to remove the effects of serial correlation present in the dataset, due to the nature of weekly sampling replicates. A single outlier identified through residual plotting was also removed to account for possible measurement error or an anomalous observation likely to be highly influential on the overall fit of the model.

3. RESULTS

Within the near-surface waters (i.e. 12 m), *LA* measurements made by the HyperPro and TDLRs were positively correlated with a RMSE of 0.56 and MAPE of 17.4% (Fig. 2), although they varied among TDLRs (Table 1). LA_{TDLR} were positively correlated with chl *a* and were slightly variable, but similar to that of LA_{HP}, supporting the use of the bio-optical model for TDLR data. While correlations with both LA_{TDLR} and LA_{HP} were strong, F_{chl} was more correlated with LA_{TDLR}. It is possible that this difference was a result of TDLRs and the fluorometer being simultaneously deployed on the CTD. F_{chl} was more strongly correlated with LA_{HP} and LA_{TDLR} than chl *a*, which may have partly been due to the relatively greater amount of data available within the water column used to calculate the per meter average. However, chl *a* and F_{chl} were highly correlated, confirming that weighted averages of chl *a* provide a good representation of the vertically integrated chl *a* over time and are useful for development of the bio-optical model as well as its application to TDLR data. $A_{CDOM}(465)$ was more strongly correlated with LA_{HP} than with LA_{TDLR}, which may have been due to the use of only a single wavelength for $a_{CDOM}(465)$ and LA_{HP} data. The correlations of $a_{CDOM}(465)$ with LA_{HP} and chl *a* with LA_{HP} were similar, suggesting that although the contribution of a_{CDOM} at 465 nm is expected to be low compared to at shorter wavelengths, it may still be influential on the development of a bio-optical model.

The most parsimonious bio-optical model for the estimation of chl *a* included both LA_{HP} and season as a fixed effect and was selected using the Akaike information criterion (Table 2, Fig. 3). The relationship between chl *a* and LA_{HP} in fall (model intercept), spring, and summer did not significantly differ from one another, but in winter, the observed chl *a* for a given LA_{HP} was lower than in other seasons (Table 3).

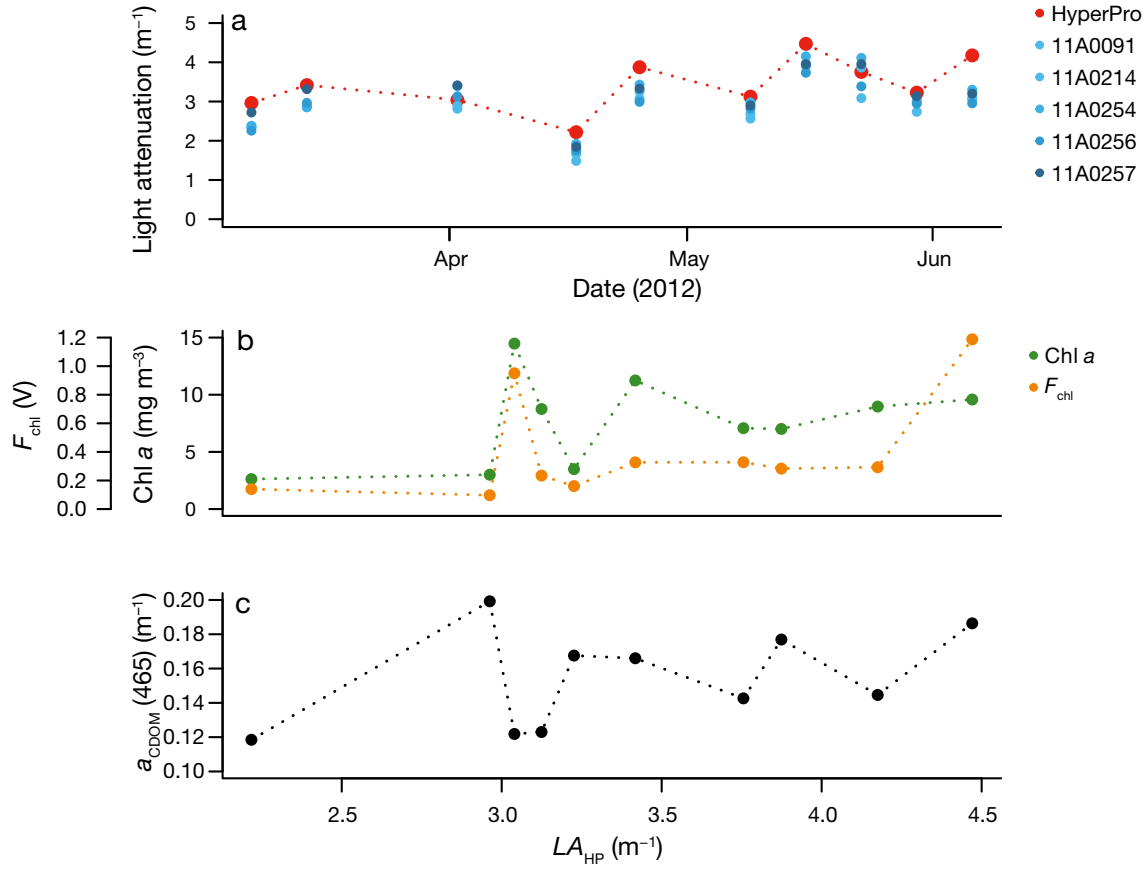

Fig. 2. (a) Light attenuation (m^{-1}) estimates from the HyperPro (LA_{HP}) and time–depth–light recorders (blue dots) within the near-surface depth (12 m) and (b) LA_{HP} compared to the chl *a* concentration (mg m^{-3}), chl *a* fluorescence intensity (F_{chl}; V), and (c) absorption by coloured dissolved organic matter (CDOM) at 465 nm ($a_{CDOM}(465)$; m^{-1}). Dotted lines are used to highlight comparisons between the different measurement types

Table 1. (a) Correlation coefficients among light attenuation (LA; m^{-1}) measurements made using 5 time–depth–light recorders (TDLRs) and the HyperPro and indicators of optically active constituents including chl *a* concentration (mg m^{-3}), chl *a* fluorescence intensity (F_{chl}; V), and coloured dissolved organic matter (CDOM) absorption at 465 nm ($a_{CDOM}(465)$; m^{-1}) and (b) the respective p-values

	TDLRs					HyperPro	Chl *a*	F_{chl}
	11A0091	11A0214	11A0254	11A0256	11A0257			
(a) Correlation coefficients								
11A0091								
11A0214	0.95							
11A0254	0.90	0.95						
11A0256	0.95	0.87	0.95					
11A0257	0.90	0.85	0.90	0.99				
HyperPro	0.92	0.89	0.77	0.71	0.67			
Chl *a*	0.52	0.37	0.45	0.66	0.62	0.43		
F_{chl}	0.81	0.71	0.78	0.93	0.90	0.62	0.84	
$a_{CDOM}(465)$	0.32	0.35	0.21	0.18	0.12	0.42	−0.11	−0.067
(b) p-values								
HyperPro	<0.001	<0.001	0.01	0.02	0.03			
Chl *a*	0.13	0.29	0.19	0.04	0.05	0.21		
F_{chl}	<0.001	0.02	0.01	<0.001	<0.001	0.05	<0.001	
$a_{CDOM}(465)$	0.37	0.33	0.56	0.63	0.75	0.23	0.75	0.85

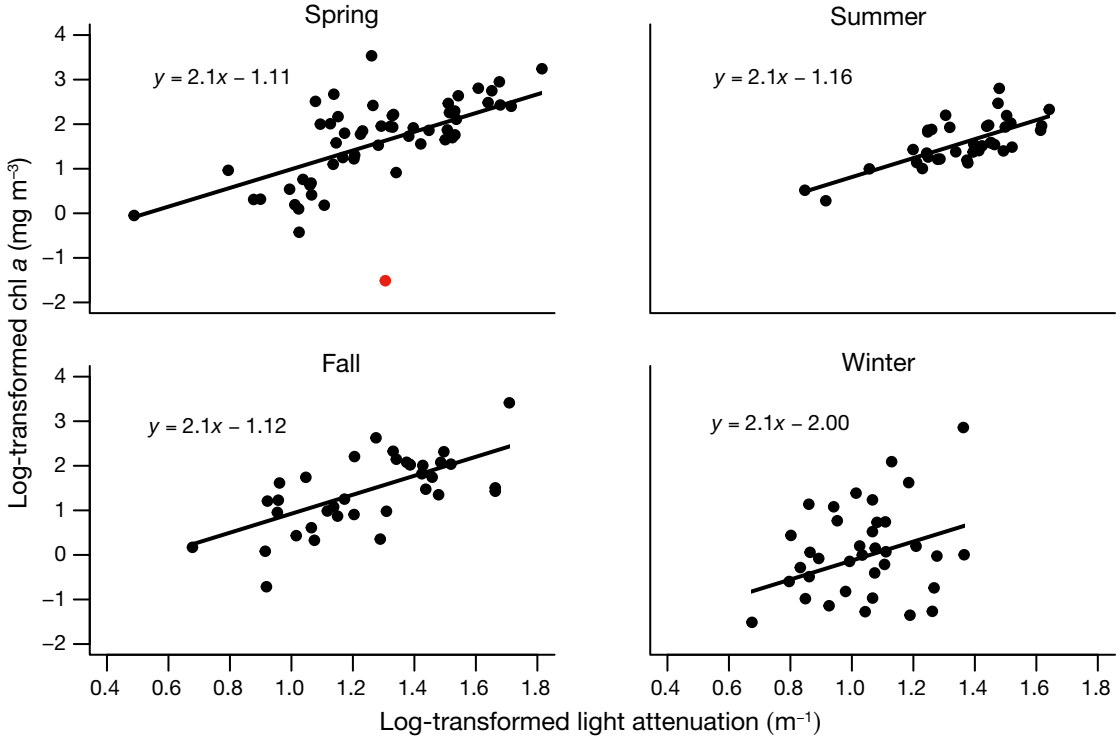

Fig. 3. Generalized least squares regression of light attenuation (m^{-1}) against chl *a* concentration (mg m^{-3}) within the near-surface depth (12 m) between 2010 and 2015 (n = 164). Both axes have been log-transformed and a continuous first-order autoregressive structure was specified; an outlier not included in the analysis is highlighted in red (n = 1)

4. DISCUSSION

The results of our replicated experiment show that it is possible to develop a bio-optical model for the estimation of chl *a* using *LA* measurements obtained from standard oceanographic instruments for the optically complex conditions of the Bedford Basin. Our results also show that *LA* measurements made using

Table 2. Determination of the most parsimonious bio-optical model (**bold**) by generalized least squares regression using the Akaike information criterion (AIC). Predictors include light attenuation (*LA*) and season (S)

Candidate models	AIC	ΔAIC
***LA* + S**	**304.69**	**0**
LA + S + *LA*:S	308.66	3.97
LA	320.29	15.60
S	377.76	57.46
~1	396.88	19.12

Table 3. Coefficient results from the most parsimonious bio-optical model. Predictors include light attenuation (*LA*) and season (S)

Variable	Coefficient ± SE	p-value
Intercept	−1.12 ± 0.311	<0.001
LA	2.07 ± 0.215	<0.0001
S (Spring)	0.003 ± 0.207	0.99
S (Summer)	−0.05 ± 0.214	0.83
S (Winter)	−0.89 ± 0.219	<0.001

TDLRs are highly correlated with those of the HyperPro. Thus, it should be possible for instrumented grey seals, and potentially other large-bodied diving species, to collect fine-scale depth-integrated chl *a* data throughout the year in areas of continental shelves where sample coverage is consistently low or lacking. The estimation of chl *a* concentration concurrently with animal locations allows for inferences to be made about the influence of phytoplankton distribution and abundance on the movements of large marine predators. Although we expect the presence of exogenous sources of CDOM to be significant in this Case 2 system, our bio-optical model demonstrates that its influence on *LA* is relatively stable over time and can be accounted for when using chl *a* alone.

4.1. Bio-optical model

The analysis of subsurface chl *a* should be performed above the depth that is considered to represent most of the phytoplankton biomass within the water column (Ross et al. 2017), typically either the euphotic zone depth (Jaud et al. 2012) or MLD (O'Toole et al. 2014). In studies involving animal-borne data, a single standardized depth has commonly been used on all profiles. The depth selected is particularly important for the Scotian Shelf, where the MLD is seasonally far deeper than the euphotic zone depth (Ross et al. 2017). Although we would have ideally extended our bio-optical model to the MLD and validated *LA* measurements to this depth, these data were not available. Estimates of the MLD using CTD data were below the 12 m near-surface depth on all 10 sampling dates that it was calculated, such that phytoplankton should be present to at least the depth where the model was formed. Although not all of the phytoplankton are represented in the bio-optical model, the relationship between chl *a* and *LA* should not change regardless of the depth to which data are collected.

We used HyperPro measurements at only the peak sensitivity of TDLRs resulting in a bio-optical model suitable for making inferences from data collected by grey seals, and potentially other large marine vertebrates fitted with similar data-loggers. The inclusion of additional spectral data collected at the half band width wavelengths (i.e. 420 and 470 nm) degraded the quality of the relationship between the HyperPro and TDLRs. If LA_{TDLR} were influenced by the attenuation of light by phytoplankton at lower wavelengths, it would be expected that LA_{TDLR} would be greater than LA_{HP}, as it was measured only at 465 nm. However, LA_{HP} was greater than some or all LA_{TDLR} measurements on all dates of the study. This suggests that if this approach were to be adopted more widely, further validation of the spectral sensitivity of TDLRs should be conducted. For this reason, measurements of a_{CDOM} were also restricted to the peak sensitivity of TDLRs. Although hyperspectral data were available, we aimed to assess whether the absorption by exogenous CDOM would potentially obscure the relationship between chl *a* and *LA* at wavelengths TDLRs are sensitive to. Estimation of *LA* by linear regression is increasingly accurate at greater depths (Lee et al. 2005b). Plots of *LL* profiles collected by the HyperPro and TDLRs demonstrated that TDLRs were in fact more sensitive to low light levels encountered at-depth (Fig. 4). Measurements made below these depths, occurring at *LL* of approximately 150, should be regarded as electronic noise (pers. comm. MEOPAR). On all 10 sampling dates, the maximum depth that *LL* change was detected by the HyperPro fell below the near-surface depth but above the MLD, such that validation could not be made at greater depths. An exploratory analysis to depths where the HyperPro showed reduced sensitivity indicated that the RMSE and MAPE improved with depth and correlations remained strong but were less variable among TDLRs. This suggests that when the model is applied to TDLR data at greater depths *in situ*, TDLR data should be more

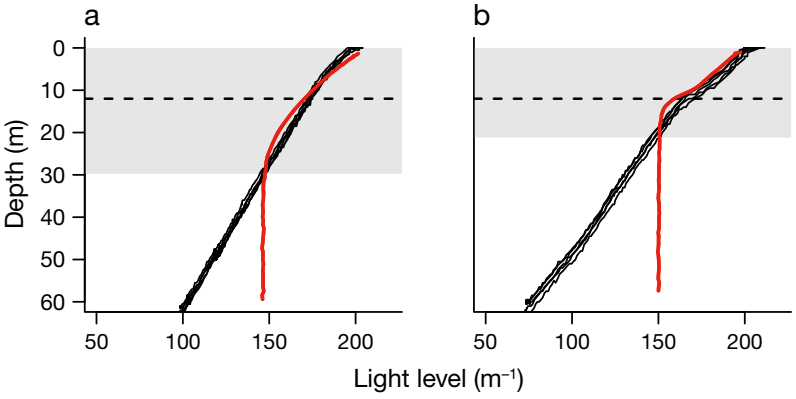

Fig. 4. Light level profiles produced using time–depth–light recorders (black) and the HyperPro (red) on (a) March 7, 2012 and (b) April 2, 2012, highlighting the limitation of the HyperPro sensitivity at low light levels (shaded) with the near-surface depth of 12 m (dashed line) for reference

similar to what would be expected for the HyperPro and the results of the predictive model may be more accurate.

Phytoplankton biomass is lowest in winter, as the water column is completely mixed, and both temperature and light intensity are reduced (Longhurst 1995, Li et al. 2006). However, remote sensing data on the Scotian Shelf indicate that while chl *a* values are low throughout winter, they are at a minimum in summer (Fuentes-Yaco et al. 2015), suggesting that pigment packaging and other physiological differences may be seasonally specific. Together with evidence for seasonality in community composition and species abundances (Li et al. 2006, Craig et al. 2015), this provides support for inclusion of season as an explanatory variable in our model. While the pattern of seasonality in phytoplankton abundance in the Bedford Basin and across the Scotian Shelf are generally consistent (Li et al. 2006), chl *a* values in the Bedford Basin tend to span a wider range (Li et al. 2006, Li 2014). On the eastern Scotian Shelf, chl *a* typically ranges from 0.5 to 3.0 mg m^{-3} and is estimated with a retrieval error of 35% (Zhai et al. 2011, Fuentes-Yaco et al. 2015). Measurements of chl *a* in our study were consistent with previous studies conducted in the Bedford Basin (Li & Dickie 2001, Ji et al. 2007). Chl *a* data included in the bio-optical model ranged between 0.22 and 34.28 mg m^{-3} with a median value of 4.07 mg m^{-3}, suggesting the bio-optical model is well suited for this ecosystem but can accommodate a wider range of chl *a* that may be present at fine spatio–temporal scales. A single outlier was removed from the data in spring. This may have been due to unseasonably low chl *a* concentrations relative to the observed LA_{HP} (e.g. changes in the community composition during blooms) or where the influence of anomalous CDOM were present (e.g. high output from the Sackville River). These data were removed to better reflect the typical conditions of the region, and perhaps those that would be expected for the Scotian Shelf which does not experience these anomalous inputs. Although the influence of CDOM in this system is relatively strong, it was also otherwise relatively constant within our study site, as we were able to develop a seasonally specific linear models despite the influence of CDOM on the attenuation of light.

4.2. Application of the bio-optical model to the adjacent Scotian Shelf

An assumption of our bio-optical model is that the optical conditions of the Bedford Basin are reasonably representative of those that grey seals would encounter in Case 2 components of the Scotian Shelf. We believe that this is a reasonable assumption, but we acknowledge that this assumption will need further evaluation. Waters of the Scotian Shelf can be traced to 2 main sources: the cooler, fresher water of the Gulf of St. Lawrence and the warmer, more saline water from the shelf-break (Smith & Schwing 1991, Loder et al. 1998, Han et al. 1999). Water originating from the Gulf of St. Lawrence becomes trapped along the coast of Nova Scotia to become the Nova Scotia Current (Dever et al. 2016). Near-surface waters of the Bedford Basin included in the formation of this model consist largely of seawater stemming from the Scotian Shelf with a landward jet centered at 5 m depth, in addition to freshwater inputs at the surface (i.e. <5 m) from precipitation and outflow from the Sackville River (Shan et al. 2011, Shan & Sheng 2012). The outflow of the Gulf of St. Lawrence also extends southwestward across the eastern Scotian Shelf, forming the upper layer, reaching between 30 and 40 m in summer and 100 m depth in winter (Han et al. 1999). The upper layer of the Scotian Shelf is predominantly made up of water originating from the Gulf of St. Lawrence (Dever et al. 2016). As such, these waters are rich in CDOM, which can be visualised through remote sensing data (Laliberté et al. 2018). Telemetry data have shown that grey seals predominantly inhabit the eastern Scotian Shelf and lower Gulf of St. Lawrence, particularly during summer and fall prior to the breeding season, when most

data are available (Breed et al. 2006, Lidgard et al. 2014). Individuals spend most of their time at sea foraging, during which movements are concentrated over shallow banks characteristic of this region, with dive depths averaging only around 50 m (Beck et al. 2003, Breed et al. 2006, 2009, Nowak 2019). For this reason, it is expected that grey seals should predominantly encounter waters stemming from the Gulf of St. Lawrence during foraging trips.

The instrumentation of grey seals and potentially other large marine vertebrates to estimate chl *a* using this bio-optical model may allow for the *in situ* monitoring of phytoplankton biomass patterns throughout the year in what may be considered the most productive and ecologically interesting regions of the Scotian Shelf. In addition to their value in leading to a better understanding of the biological oceanography of this continental shelf, the collection of depth-integrated chl *a* data using animal-borne instruments may also inform studies of habitat use of large marine vertebrates (e.g. Nowak 2019).

Acknowledgements. The authors acknowledge the valuable contribution of MEOPAR and Dalhousie University for the collection and processing of data collected in the Bedford Basin. We especially thank Richard Davis and Anna Haverstock for providing access to oceanographic data from the MEOPAR program and their assistance with the interpretation and analysis of those data. This study was supported by grants to the Ocean Tracking Network (OTN) from the Natural Sciences and Engineering Research Council (NSERC) of Canada (Research Network Grant NETGP 375118-08) and the Canada Foundation for Innovation (CFI). Additional support was provided by the Department of Fisheries and Oceans (DFO) Canada, NSERC Discovery Grants to WDB and SJI, and a Nova Scotia Graduate Scholarship to BVRN.

LITERATURE CITED

Ackerman SA, Strabala KI, Menzel WP, Frey RA, Moeller CC, Gumley LE (1998) Discriminating clear sky from clouds with MODIS. J Geophys Res Atmos 103:32141–32157

Bailleul F, Authier M, Ducatez S, Roquet F, Charrassin J, Cherel Y, Guinet C (2010) Looking at the unseen: combining animal bio-logging and stable isotopes to reveal a shift in the ecological niche of a deep diving predator. Ecography 33:709–719

Baker K, Smith R (1982) Bio-optical classification and model of natural waters. 2. Limnol Oceanogr 27:500–509

Bayle S, Monestiez P, Guinet C, Nerini D (2015) Moving toward finer scales in oceanography: predictive linear functional model of chlorophyll *a* profile from light data. Prog Oceanogr 134:221–231

Beck M (2016) Defining a multi-parameter optics-based approach for estimating chlorophyll *a* concentration using ocean gliders. MSc thesis, Dalhousie University, Halifax

Beck CA, Bowen WD, McMillan JI, Iverson SJ (2003) Sex differences in the diving behaviour of a size-dimorphic capital breeder: the grey seal. Anim Behav 66:777–789

Behrenfeld M, Falkowski P (1997) Photosynthetic rates derived from satellite-based chlorophyll concentration. Limnol Oceanogr 42:1–20

Behrenfeld MJ, Westberry TK, Boss ES, O'Malley RT and others (2009) Satellite-detected fluorescence reveals global physiology of ocean phytoplankton. Biogeosciences 6:779–794

Behrenfeld MJ, O'Malley RT, Boss ES, Westberry TK and others (2016) Revaluating ocean warming impacts on global phytoplankton. Nat Clim Chang 6:323–330

Blain S, Renaut S, Xing X, Claustre H, Guinet C (2013) Instrumented elephant seals reveal the seasonality in chlorophyll and light-mixing regime in the iron-fertilized Southern Ocean. Geophys Res Lett 40:6368–6372

Blondeau-Patissier D, Gower JFR, Dekker AG, Phinn SR, Brando VE (2014) A review of ocean color remote sensing methods and statistical techniques for the detection, mapping and analysis of phytoplankton blooms in coastal and open oceans. Prog Oceanogr 123:123–144

Breed GA, Bowen WD, McMillan JI, Leonard ML (2006) Sexual segregation of seasonal foraging habitats in a non-migratory marine mammal. Proc R Soc B 273: 2319–2326

Breed GA, Jonsen ID, Myers RA, Bowen WD, Leonard ML (2009) Sex-specific, seasonal foraging tactics of adult grey seals (*Halichoerus grypus*) revealed by state-space analysis. Ecology 90:3209–3221

Bricaud A, Morel A, Prieur L (1981) Absorption by dissolved organic matter of the sea (yellow substance) in the UV and visible domains. Limnol Oceanogr 26:43–53

Bundy A, Themelis D, Sperl J, den Heyer CE (2014) Inshore Scotian Shelf ecosystem overview report: status and trends. DFO Can Sci Advis Sec Res Doc 2014/065.

Campagna C, Piola AR, Marin MR, Lewis M, Zajaczkoyski U, Fernandez T (2007) Deep divers in shallow seas: southern elephant seals on the Patagonian shelf. Deep Sea Res I 54:1792–1814

Craig SE, Thomas H, Jones CT, Li WK, Greenan BJ, Shadwick EH, Burt WJ (2015) The effect of seasonality in phytoplankton community composition on CO_2 uptake on the Scotian Shelf. J Mar Syst 147:52–60

Cullen J (1982) The deep chlorophyll maximum: comparing vertical profiles of chlorophyll *a*. Can J Fish Aquat Sci 39:791–803

Cullen J, Lewis M (1995) Biological processes and optical measurements near the sea surface: some issues relevant to remote sensing. J Geophys Res Oceans 100: 13255–13266

Darecki M, Weeks A, Sagan S, Kowalczuk P, Kaczmarek S (2003) Optical characteristics of two contrasting Case 2 waters and their influence on remote sensing algorithms. Cont Shelf Res 23:237–250

de Boyer Montégut C, Madec G, Fischer A, Lazar A, Iudicone D (2004) Mixed layer depth over the global ocean: an examination of profile data and a profile-based climatology. J Geophys Res Oceans 109:C12003

Dever M, Hebert D, Greenan BJW, Sheng J, Smith PC (2016) Hydrography and coastal circulation along the Halifax Line and the connections with the Gulf of St. Lawrence. Atmos-Ocean 54:199–217

Devred E, Fuentes-Yaco C, Sathyendranath S, Caverhill C and others (2005) A semi-analytic seasonal algorithm to

retrieve chlorophyll-a concentration in the Northwest Atlantic Ocean from SeaWiFS data. Indian J Geo-Mar Sci 34:356–367

Falkowski PG, Barber RT, Smetacek V (1998) Biogeochemical controls and feedbacks on ocean primary production. Science 281:200–206

Field CB, Behrenfeld MJ, Randerson JT, Falkowski P (1998) Primary production of the biosphere: integrating terrestrial and oceanic components. Science 281:237–240

Friedl MA, Sulla-Menashe D, Tan B, Schneider A, Ramankutty N, Sibley A, Huang X (2010) MODIS Collection 5 global land cover: algorithm refinements and characterization of new datasets. Remote Sens Environ 114:168–182

Fuentes-Yaco C, King M, Li WKW (2015) Mapping areas of high phytoplankton biomass in the offshore component of the Scotian Shelf Bioregion: a remotely-sensed approach. DFO Can Sci Advis Sec Res Doc 2015/036

Greenberg D, Loder J, Shen Y, Lynch D, Naimie C (1997) Spatial and temporal structure of the barotropic response of the Scotian Shelf and Gulf of Maine to surface wind stress: a model-based study. J Geophys Res 102:20897–20915

Guinet C, Xing X, Walker E, Monestiez P and others (2013) Calibration procedures and first dataset of Southern Ocean chlorophyll *a* profiles collected by elephant seals equipped with a newly developed CTD-fluorescence tags. Earth Syst Sci Data 5:15–29

Hammill MO, den Heyer CE, Bowen WD, Lang SLC (2017) Grey seal population trends in Canadian waters, 1960–2016 and harvest advice. DFO Can Sci Advis Sec Res Doc 2017/052

Han G, Loder J, Smith P (1999) Seasonal-mean hydrography and circulation in the Gulf of St. Lawrence and on the eastern Scotian and southern Newfoundland shelves. J Phys Oceanogr 29:1279–1301

Helms JR, Stubbins A, Ritchie JD, Minor EC, Kieber DJ, Mopper K (2008) Absorption spectral slopes and slope ratios as indicators of molecular weight, source, and photobleaching of chromophoric dissolved organic matter. Limnol Oceanogr 53:955–969

Hindell MA, McMahon CR, Bester MN, Boehme L and others (2016) Circumpolar habitat use in the southern elephant seal: implications for foraging success and population trajectories. Ecosphere 7:e01213

Hooker SK, Boyd IL (2003) Salinity sensors on seals: use of marine predators to carry CTD data loggers. Deep Sea Res I 50:927–939

Jaud T, Dragon A, Vacquié-Garcia J, Guinet C (2012) Relationship between chlorophyll *a* concentration, light attenuation and diving depth of the southern elephant seal *Mirounga leonina*. PLOS ONE 7:e47444

Ji R, Davis CS, Chen C, Townsend DW, Mountain DG, Beardsley RC (2007) Influence of ocean freshening on shelf phytoplankton dynamics. Geophys Res Lett 34: L24607

Kirk KTO (1994) Light and photosynthesis in aquatic ecosystems. Cambridge University Press, Cambridge

Laliberté J, Larouche P, Devred E, Craig S (2018) Chlorophyll-a concentration retrieval in the optically complex waters of the St. Lawrence Estuary and Gulf using principal component analysis. Remote Sens 10:265

Lander ME, Lindstrom T, Rutishauser M, Franzheim A, Holland M (2015) Development and field testing a satellite-linked fluorometer for marine vertebrates. Anim Biotelem 3:40

Lee Z, Darecki M, Carder KL, Davis CO, Stramski D, Rhea WJ (2005a) Diffuse attenuation coefficient of downwelling irradiance: an evaluation of remote sensing methods. J Geophys Res Oceans 110:C02017

Lee Z, Du K, Arnone R (2005b) A model for the diffuse attenuation coefficient of downwelling irradiance. J Geophys Res Oceans 110:C02016

Lewis MR, Platt T (1982) Scales of variability in estuarine ecosystems. In: Kennedy VS (ed) Estuarine comparisons. Academic Press, New York, NY, p 3–20

Li WKW (2014) The state of phytoplankton and bacterioplankton at the Compass Buoy Station: Bedford Basin Monitoring Program 1992–2013. Can Tech Rep Hydrogr Ocean Sci 304

Li WKW, Dickie PM (2001) Monitoring phytoplankton, bacterioplankton, and virioplankton in a coastal inlet (Bedford Basin) by flow cytometry. Cytometry 44:236–246

Li WKW, Harrison WG (2008) Propagation of an atmospheric climate signal to phytoplankton in a small marine basin. Limnol Oceanogr 53:1734–1745

Li WKW, Harrison WG, Head EJ (2006) Coherent assembly of phytoplankton communities in diverse temperate ocean ecosystems. Proc R Soc B 273:1953–1960

Li WKW, Lewis MR, Harrison WG (2010) Multiscalarity of the nutrient–chlorophyll relationship in coastal phytoplankton. Estuaries Coasts 33:440–447

Lidgard DC, Bowen WD, Jonsen ID, Iverson SJ (2014) Predator-borne acoustic transceivers and GPS tracking reveal spatiotemporal patterns of encounters with acoustically tagged fish in the open ocean. Mar Ecol Prog Ser 501: 157–168

Loder JW, Petrie B, Gawarkiewicz G (1998) The coastal ocean off northeastern North America: a large-scale view. In: Robinson AR, Brink KH (ed) The sea, Vol 11. Wiley, New York, NY, p 105–133

Longhurst A (1995) Seasonal cycles of pelagic production and consumption. Prog Oceanogr 36:77–167

Moore TS, Campbell JW, Dowell MD (2009) A class-based approach to characterizing and mapping the uncertainty of the MODIS ocean chlorophyll product. Remote Sens Environ 113:2424–2430

Moore JK, Fu W, Primeau F, Britten GL and others (2018) Sustained climate warming drives declining marine biological productivity. Science 359:1139–1143

Morel A, Maritorena S (2001) Bio-optical properties of oceanic waters: a reappraisal. J Geophys Res Oceans 106:7163–7180

Morel A, Prieur L (1977) Analysis of variations in ocean color. Limnol Oceanogr 22:709–722

Morel A, Gentili B, Chami M, Ras J (2006) Bio-optical properties of high chlorophyll Case 1 waters and of yellow-substance-dominated Case 2 waters. Deep Sea Res I 53:1439–1459

Moses WJ, Gitelson AA, Berdnikov S, Povazhnyy V (2009) Estimation of chlorophyll-a concentration in case II waters using MODIS and MERIS data — successes and challenges. Environ Res Lett 4:045005

Nowak BVR (2019) *In situ* measurements by instrumented grey seals (*Halichoerus grypus*) reveal fine-scale oceanographic properties and environmental influences on movement patterns. MSc thesis, Dalhousie University, Halifax

O'Reilly JE, Maritorena S, Mitchell BG, Siegel DA and others (1998) Ocean color chlorophyll algorithms for SeaWiFS. J Geophys Res Oceans 103:24937–24953

O'Toole MD, Lea M, Guinet C, Hindell MA (2014) Estimating trans-seasonal variability in water column biomass for a highly migratory, deep diving predator. PLOS ONE 9:e113171

Padman L, Costa DP, Bolmer ST, Goebel ME and others (2010) Seals map bathymetry of the Antarctic continental shelf. Geophys Res Lett 37:L21601

Petrie B, Yeats P, Strain P (1999) Nitrate, silicate and phosphate atlas for the Scotian Shelf and the Gulf of Maine. Can Tech Rep Hydrogr Ocean Sci 203

Platt T, Prakash A, Irwin B (1972) Phytoplankton nutrients and flushing of inlets on the coast of Nova Scotia. Nat Can 99:253–261

R Core Team (2018) R: a language and environment for statistical computing. R Foundation for Statistical Computing, Vienna. https://www.R-project.org/

Riser SC, Freeland HG, Roemmich D, Wijffels S and others (2016) Fifteen years of ocean observations with the global Argo array. Nat Clim Chang 6:145–153

Roquet F, Williams G, Hindell MA, Harcourt R and others (2014) A Southern Indian Ocean database of hydrographic profiles obtained with instrumented elephant seals. Sci Data 1:140028

Ross T, Craig SE, Comeau A, Davis R, Dever M, Beck M (2017) Blooms and subsurface phytoplankton layers on the Scotian Shelf: insights from profiling gliders. J Mar Syst 172:118–127

Sarmiento J, Hughes T, Stouffer R, Manabe S (1998) Simulated response of the ocean carbon cycle to anthropogenic climate warming. Nature 393:245–249

Shan S, Sheng J (2012) Examination of circulation, flushing time and dispersion in Halifax Harbour of Nova Scotia. Water Qual Res J Canada 47:353–374

Shan S, Sheng J, Thompson KR, Greenberg DA (2011) Simulating the three-dimensional circulation and hydrography of Halifax Harbour using a multi-nested coastal ocean circulation model. Ocean Dyn 61:951–976

Siegel D, Maritorena S, Nelson N, Behrenfeld M, McClain C (2005) Colored dissolved organic matter and its influence on the satellite-based characterization of the ocean biosphere. Geophys Res Lett 32:L20605

Simmons SE, Tremblay Y, Costa DP (2009) Pinnipeds as ocean-temperature samplers: calibrations, validations, and data quality. Limnol Oceanogr Methods 7:648–656

Smith R, Baker K (1978) Optical classification of natural waters. Limnol Oceanogr 23:260–267

Smith P, Schwing F (1991) Mean circulation and variability on the eastern Canadian continental-shelf. Cont Shelf Res 11:977–1012

Song H, Ji R, Stock C, Wang Z (2010) Phenology of phytoplankton blooms in the Nova Scotian Shelf–Gulf of Maine region: remote sensing and modeling analysis. J Plankton Res 32:1485–1499

Stabeno PJ, Schumacher JD, Davis RF, Napp JM (1998) Under-ice observations of water column temperature, salinity and spring phytoplankton dynamics: Eastern Bering Sea shelf. J Mar Res 56:239–255

Teo SLH, Kudela RM, Rais A, Perle C, Costa DP, Block BA (2009) Estimating chlorophyll profiles from electronic tags deployed on pelagic animals. Aquat Biol 5:195–207

Thompson D, Hammond P, Nicholas K, Fedak M (1991) Movements, diving and foraging behavior of gray seals (*Halichoerus grypus*). J Zool (Lond) 224:223–232

Tuszynski J (2014) Tools: moving window statistics, GIF, Base64, ROC AUC, etc. R Package Version 1.17.1.2. https://CRAN.R-project.org/package=caTools

Vacquié-Garcia J, Mallefet J, Bailleul F, Picard B, Guinet C (2017) Marine bioluminescence: measurement by a classical light sensor and related foraging behavior of a deep diving predator. Photochem Photobiol 93:1312–1319

Welschmeyer NA (1994) Fluorometric analysis of chlorophyll a in the presence of chlorophyll b and pheopigments. Limnol Oceanogr 39:1985–1992

Wynn RB, Huvenne VA, Le Bas TP, Murton BJ and others (2014) Autonomous underwater vehicles (AUVs): their past, present and future contributions to the advancement of marine geoscience. Mar Geol 352:451–468

Xie H, Aubry C, Bélanger S, Song G (2012) The dynamics of absorption coefficients of CDOM and particles in the St. Lawrence estuarine system: biogeochemical and physical implications. Mar Chem 128:44–56

Xing X, Claustre H, Blain S, D'Ortenzio F, Antoine D, Ras J, Guinet C (2012) Quenching correction for in vivo chlorophyll fluorescence acquired by autonomous platforms: a case study with instrumented elephant seals in the Kerguelen region (Southern Ocean). Limnol Oceanogr Methods 10:483–495

Zhai L, Platt T, Tang C, Sathyendranath S, Hernández Walls R (2011) Phytoplankton phenology on the Scotian Shelf. ICES J Mar Sci 68:781–791

Editorial responsibility: Steven Lohrenz, New Bedford, Massachusetts, USA
Reviewed by: T. Keates and 3 anonymous referees

Submitted: October 12, 2020
Accepted: August 30, 2021
Proofs received from author(s): November 18, 2021